*Erschienen in: Philosophical Transactions of the Royal Society of London, Series A : Mathematical, Physical and Engineering Sciences ; 376 (2018), 2125. - 20150229*
*https://dx.doi.org/10.1098/rsta.2015.0229*

# Non-equilibrium charge and spin transport in superconducting–ferromagnetic–superconducting point contacts

C. Holmqvist[1], W. Belzig[2] and M. Fogelström[3]

[1]Department of Physics, Norwegian University of Science and Technology, 7491 Trondheim, Norway
[2]Fachbereich Physik, Universität Konstanz, 78457 Konstanz, Germany
[3]Department of Microtechnology and Nanoscience - MC2, Chalmers University of Technology, 412 96 Göteborg, Sweden

**Subject Areas:**
mesoscopics, low-temperature physics, nanotechnology, spintronics

**Keywords:**
superconductivity, magnetism, Andreev bound states, Landau–Lifshitz–Gilbert equation, multiple Andreev reflection, Shapiro steps

**Author for correspondence:**
M. Fogelström
e-mail: mikael.fogelstrom@chalmers.se

The conventional Josephson effect may be modified by introducing spin-active scattering in the interface layer of the junction. Here, we discuss a Josephson junction consisting of two s-wave superconducting leads coupled over a classical spin that precesses with the Larmor frequency due to an external magnetic field. This magnetically active interface results in a time-dependent boundary condition with different tunnelling amplitudes for spin-up and -down quasiparticles and where the precession produces spin-flip scattering processes. As a result, the Andreev states develop sidebands and a non-equilibrium population that depend on the details of the spin precession. The Andreev states carry a steady-state Josephson charge current and a time-dependent spin current, whose current–phase relations could be used to characterize the precessing spin. The spin current is supported by spin-triplet correlations induced by the spin precession and creates a feedback effect on the classical spin in the form of a torque that shifts the precession frequency. By applying a bias voltage, the Josephson frequency adds another complexity to the situation and may create resonances together

with the Larmor frequency. These Shapiro resonances manifest as torques and, under suitable conditions, are able to reverse the direction of the classical spin in sub-nanosecond time. Another characteristic feature is the subharmonic gap structure in the DC charge current displaying an even–odd effect attributable to precession-assisted multiple Andreev reflections.

This article is part of the theme issue 'Andreev bound states'.

## 1. Introduction

Interesting spin phenomena may occur when ferromagnets are combined with superconductors ([1,2] and references therein). Cooper pairs in a conventional superconductor have spin-singlet pairing which, if the superconductor is interfaced with a ferromagnet, extend into the ferromagnet. However, the exchange field inside the ferromagnet tries to align the two spins of the Cooper pairs and hence breaks the Cooper pairs apart, resulting in a rapid decay of the superconducting correlations inside the ferromagnet. For the same reasons, the critical current of a Josephson junction with a ferromagnetic layer sandwiched between the two superconductors decays rapidly with increasing thickness of the ferromagnetic layer [3–6]. On the other hand, if weak ferromagnetic interfaces with magnetization directions differing from the magnetization direction of the ferromagnetic layer are inserted, the spin-singlet correlations may be transformed into spin-triplet correlations which can survive over a long range within the ferromagnetic layer [7–11]. As a result of this non-collinear magnetization of the ferromagnetic layer, the critical current decays similar to a supercurrent in a non-magnetic metal with increasing junction length [12,13]. So far, the existence of spin-triplet correlations has been measured in this indirect way. A more direct way of detecting the spin-triplet correlations would be to measure the effects of the spin on the triplet correlations, e.g. by using phenomena explored in conventional spintronics such as spin-transfer torques and other means for creating magnetization dynamics effects or magnetization switching. There has been theoretical work done in this direction [14–16] using approaches based on the Bogoliubov–de Gennes equations [17–21] and Green's function methods [22–27] as well as some experimental work investigating the coupling between the dynamics of magnetic moments and Josephson currents [28,29], but to our knowledge there has been no experimental investigation of the coupling between magnetization dynamics and induced triplet correlations. This is a crucial step in developing superconducting spintronics applications [2]. In this article, we will review recent work on how magnetization dynamics of a nanomagnet couple to the induced spin-triplet correlations associated with the charge and spin Josephson effects, and discuss how the dynamic interactions between the induced spin-triplet correlations and the nanomagnet lead to non-equilibrium transport properties that can be used to probe the induced triplet correlations directly.

## 2. Quasi-classical model

Consider two ordinary Bardeen–Cooper–Schrieffer (BCS) s-wave superconductors, with a phase difference $\varphi$, coupled over a nanomagnet as depicted in figure 1*a*. The nanomagnet may be a magnetic molecule or a magnetic nanoparticle, which we will treat as a classical spin, $\boldsymbol{S}$, with magnetic moment $\boldsymbol{\mu} = \gamma \boldsymbol{S}$, and the gyromagnetic ratio $\gamma$. The nanoparticle supports a few conduction channels when placed between the two metallic leads. If the nanomagnet is subjected to an external magnetic field, $\boldsymbol{H}$, it will precess when the effective field is applied at an angle, $\vartheta$, relative to the spin. $\boldsymbol{H}$ is an effective field that includes any r.f. fields needed to maintain precession, crystal anisotropy fields and demagnetization effects. The spin and the effective magnetic field couple via a Zeeman term, $\mathcal{H}_B = -\gamma \boldsymbol{S}(t) \cdot \boldsymbol{H}$. At finite tilt angle, $\vartheta$, the spin precesses with the Larmor frequency, $\omega_{\mathrm{L}} = \gamma H$, where $H = |\boldsymbol{H}|$ is the magnitude of the effective field. The spin dynamics are described by the Landau–Lifshitz–Gilbert equation of motion [30,31]

$$\frac{\mathrm{d}\boldsymbol{S}}{\mathrm{d}t} = -\gamma \boldsymbol{S}(t) \times \boldsymbol{H} + \boldsymbol{\tau}(t), \tag{2.1}$$

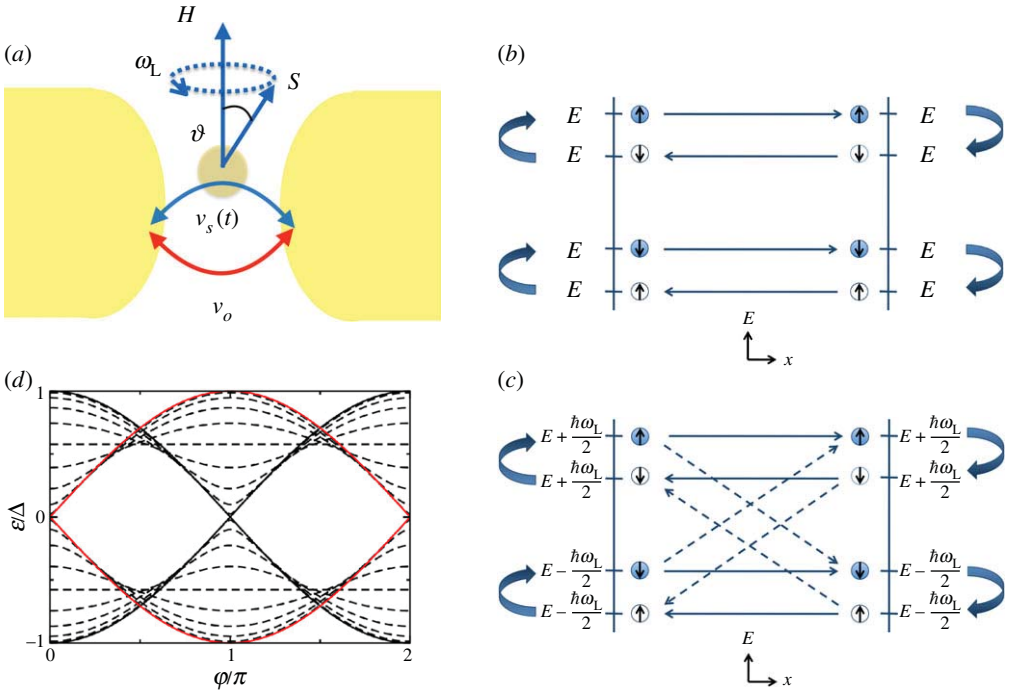


**Figure 1.** (*a*) Two superconducting leads are coupled over the spin of a nanomagnet. The tunnel junction is characterized by the hopping amplitudes $v_o$ and $v_s(t)$, where $v_o$ is the spin-independent tunnelling and $v_s(t)$ is the phenomenological time-dependent coupling generated by the nanomagnet, whose spin precesses with the frequency $\omega_L$ at the cone angle $\vartheta$. (*b*) The schematics of conventional Andreev scattering between two superconductors at phase difference $\varphi$. Constructive interference occurs at a phase-dependent energy $\varepsilon(\varphi)$ defining two energy-degenerate Andreev levels. (*c*) In addition to the spin-conserving tunnelling (solid lines), the dynamics of the spin allows for tunnelling processes with spin-flip scattering combined with an absorption or emission of the energy $\hbar\omega_L$ (dashed lines). The combination of these tunnelling processes results in a lifting of the spin degeneracy of the Andreev levels in (*b*) and the appearance of time-dependent spin-triplet pairing amplitudes. (*d*) For a junction with a static spin, the Andreev level spectrum's dependence on phase may be modified from a 0 junction, $v_o > v_s$, to a $\pi$ junction, $v_o < v_s$. The black full line is $(v_o, v_s) = (1, 0)$ and the red line is $(v_o, v_s) = (0, 1)$. The dashed lines span between these two limits in increments of 0.1. (Online version in colour.)

where the first term on the right-hand side is the torque produced by the effective field and the second term, $\boldsymbol{\tau}(t)$, is a torque that collects effects caused by the mutual coupling between the precessing nanomagnet and the superconducting quasi-particle system.

The coupling of the motion of the spin and the quasi-particle tunnelling over the spin enters via a time-dependent tunnelling term, $\hat{\mathcal{H}}_T = \hat{\psi}_L^\dagger \hat{v}_{LR}(t)\hat{\psi}_R + \text{H.C.}$, where $\hat{\psi}_\alpha$ is the usual spin-dependent Nambu spinor that describes the superconducting state in lead $\alpha = R, L$. The hopping matrix $\hat{v}_{LR}(t)\,(= \hat{v}_{RL}^\dagger(t) \equiv \hat{v}(t))$ has a spin structure that may be parametrized into a spin-independent amplitude $v_o$ and a spin-dependent amplitude $v_s(t)$. It has the following matrix structure in the combined $4 \times 4$ Nambu spin space,

$$\hat{v}_{LR}(t) = \begin{pmatrix} v_o + v_s(\boldsymbol{e}_S(t)\cdot\boldsymbol{\sigma}) & 0 \\ 0 & v_o - v_s\sigma_y(\boldsymbol{e}_S(t)\cdot\boldsymbol{\sigma})\sigma_y \end{pmatrix}. \tag{2.2}$$

We use the time-dependent unit vector, $\boldsymbol{e}_S(t)$, along $\boldsymbol{S}(t) = |\boldsymbol{S}|\boldsymbol{e}_S(t)$ and include the magnitude $|\boldsymbol{S}|$ in the spin-dependent amplitude $v_s$. Above, $\boldsymbol{\sigma} = (\sigma_x, \sigma_y, \sigma_z)$ with $\sigma_i$ being the $i$th Pauli matrix. The spin-independent amplitude and the portion of the spin matrix parallel to $\boldsymbol{H}$, $v_o + v_s\cos\vartheta(\boldsymbol{e}_z\cdot\boldsymbol{\sigma})$, describe the tunnelling amplitudes for spin-up and spin-down quasi-particles, while the portion

perpendicular to $\boldsymbol{H}$, $v_s \sin\vartheta(\cos(\omega_L t)\boldsymbol{e}_x + \sin(\omega_L t)\boldsymbol{e}_y)\cdot\boldsymbol{\sigma}$, induces time-dependent spin flips. Our model is a generalization to arbitrary tunnelling coupling of the one studied by Zhu and co-workers [22,32].

We use the quasi-classical theory of superconductivity [33–36] to solve the non-equilibrium tunnelling problem stated above. Within quasi-classical theory, interfaces are handled by the formulation of boundary conditions, which usually have been expressed as scattering problems [37–46]. In many problems, in particular when an explicit time dependence appears, we find the $t$-matrix formulation more convenient to use [47–49]. This formulation is also well suited for studying interfaces with different numbers of trajectories on either side, as is the case for normal metal–half-metal interfaces [50,51]. For a full account on how to solve the time-dependent boundary condition, we refer to our original articles [52–55].

The quasi-classical propagator in lead $\alpha$, $\check{g}_\alpha$, is a $2\times 2$ matrix in Keldysh space, denoted by the check '$\check{}$'. Each component is in turn a $4\times 4$ matrix in the combined Nambu spin space and has the general form

$$\hat{g}^{\mathrm{R,A,K}} = \begin{pmatrix} g + \boldsymbol{g}\cdot\boldsymbol{\sigma} & (f + \boldsymbol{f}\cdot\boldsymbol{\sigma})\mathrm{i}\sigma_y \\ \mathrm{i}\sigma_y(\tilde{f} + \tilde{\boldsymbol{f}}\cdot\boldsymbol{\sigma}) & \sigma_y(\tilde{g} - \tilde{\boldsymbol{g}}\cdot\boldsymbol{\sigma})\sigma_y \end{pmatrix}^{\mathrm{R,A,K}} \tag{2.3}$$

for the retarded (R), advanced (A) and Keldysh (K) components. To obtain $\check{g}_\alpha$ for a non-homogeneous system, we solve the transport equation

$$\mathrm{i}v_F\partial_x\check{g}_\alpha(\hat{p}_F) + [\check{\varepsilon} - \check{\Delta}_\alpha, \check{g}_\alpha(\hat{p}_F)]_\circ = \frac{\check{j}_\alpha\delta(x - x_c)}{(2\pi\mathrm{i})}, \tag{2.4}$$

along a trajectory $\hat{p}_F$ in lead $\alpha$. The boundary conditions for the components of $\check{g}_\alpha$ enter via a localized inhomogeneity, given by the tunnel Hamiltonian, at the position of the contact, $x_c$ [56–58]. The source term is a matrix current defined as $\check{j}_\alpha/2\pi\mathrm{i} = [\check{t}_\alpha(\hat{p}_F, \hat{p}_F), \check{g}^0_\alpha(\hat{p}_F)]_\circ$. The $\circ$-product is a matrix multiplication and convolution over common time arguments and $\check{g}_\alpha$ additionally obeys a normalization condition $\check{g}_\alpha \circ \check{g}_\alpha = -\pi^2\check{1}$. The matrix, $\check{t}_\alpha(\hat{p}_F, \hat{p}_F)$, solves the $t$-matrix equation

$$\check{t}_\alpha(t,t') = \check{\Gamma}_\alpha(t,t') + [\check{\Gamma}_\alpha \circ \check{g}^0_\alpha \circ \check{t}_\alpha](t,t'). \tag{2.5}$$

The $t$-matrix $\check{t}_\alpha$ depends on the hopping elements of equation (2.2) via a matrix $\check{\Gamma}_L(t,t')$ defined as $\check{\Gamma}_L(t,t') = [\check{v}\circ\check{g}^0_R\circ\check{v}](t,t')$ for the left side of the interface. The right-side matrix $\check{\Gamma}_R$ is correspondingly obtained from the left-side propagator $\check{g}^0_L$. Here $\check{g}^0_{L,R}$ are the bulk propagators in either lead computed without the tunnelling term. From the $t$-matrices (2.5), we calculate the full quasi-classical propagators, which can be separated into 'incoming' ($\check{g}^{\mathrm{i}}$) and 'outgoing' ($\check{g}^{\mathrm{o}}$) propagators depending on whether their trajectories lead up to or away from the interface. These propagators are given by

$$\check{g}^{\mathrm{i,o}}_\alpha(t,t') = \check{g}^0_\alpha(t,t') + [(\check{g}^0_\alpha \pm \mathrm{i}\pi\check{1})\circ\check{t}_\alpha\circ(\check{g}^0_\alpha \mp \mathrm{i}\pi\check{1})](t,t'), \tag{2.6}$$

where $\pm$ and $\mp$ refer to the incoming and outgoing propagators, respectively. The matrix currents give the charge and spin currents via

$$j^{\mathrm{c}}_\alpha(t) = \frac{e}{2\hbar}\int\frac{\mathrm{d}\varepsilon}{8\pi\mathrm{i}}\,\mathrm{Tr}[\hat{\tau}_3\hat{j}^<_\alpha(\varepsilon,t)] \tag{2.7a}$$

and

$$j^{\mathrm{s}}_\alpha(t) = \frac{1}{4}\int\frac{\mathrm{d}\varepsilon}{8\pi\mathrm{i}}\,\mathrm{Tr}[\hat{\tau}_3\hat{\boldsymbol{\sigma}}\hat{j}^<_\alpha(\varepsilon,t)], \tag{2.7b}$$

where $\hat{\tau}_3 = \mathrm{diag}(1,-1)$, $\hat{\boldsymbol{\sigma}} = \mathrm{diag}(\boldsymbol{\sigma}, -\sigma_y\boldsymbol{\sigma}\sigma_y)$ and '$\hat{}$' denotes a $4\times 4$ matrix in Nambu spin space. The lesser ($<$) propagators can be obtained as $\hat{g}^< = \frac{1}{2}(\hat{g}^{\mathrm{K}} - \hat{g}^{\mathrm{R}} + \hat{g}^{\mathrm{A}})$. The itinerant electrons generate a spin transfer torque which gives a contribution to the torque in equation (2.1) as $\boldsymbol{\tau} = \boldsymbol{j}^{\mathrm{s}}_L - \boldsymbol{j}^{\mathrm{s}}_R$.

The spin independence of $\check{g}^0_\alpha(\varepsilon)$ and the form of the hopping elements simplify the time-dependent problem. This simplification can be made due to the fact that the Keldysh–Nambu spin matrices can be factorized in spin space into generalized diagonal matrices, $\check{X}_{\mathrm{d}}$, spin-raising

matrices, $\check{X}_\uparrow$, and spin-lowering matrices, $\check{X}_\downarrow$. In general, a matrix factorized in this form has the time dependence

$$\check{X}(t,t') = (2\pi)^{-1}\int \mathrm{d}\varepsilon\, \mathrm{e}^{-\mathrm{i}\varepsilon(t-t')}[\check{X}_\mathrm{d}(\varepsilon,\omega_\mathrm{L}) + \mathrm{e}^{-\mathrm{i}\omega_\mathrm{L}t}\check{X}_\uparrow(\varepsilon,\omega_\mathrm{L}) + \mathrm{e}^{\mathrm{i}\omega_\mathrm{L}t}\check{X}_\downarrow(\varepsilon,\omega_\mathrm{L})]. \tag{2.8}$$

The matrices $\check{X}_\mathrm{d}$, $\check{X}_\uparrow$ and $\check{X}_\downarrow$ are still Keldysh–Nambu matrices and, in addition, obey the usual algebraic rules for spin matrices, i.e. $\check{X}_\uparrow \circ \check{Y}_\uparrow = \check{X}_\downarrow \circ \check{Y}_\downarrow = 0$, $\check{X}_{\downarrow,\uparrow} \circ \check{Y}_{\uparrow,\downarrow} \propto \check{Z}_\mathrm{d}$ and $\check{X}_\mathrm{d} \circ \check{Y}_{\uparrow,\downarrow} \propto \check{Z}_{\uparrow,\downarrow}$. Observables, such as the charge and spin currents above, will have the general time dependence

$$\mathcal{O}(t;\omega_\mathrm{L}) = \mathcal{O}_\mathrm{o}(\omega_\mathrm{L}) + \mathcal{O}_z(\omega_\mathrm{L})\sigma_z + \mathcal{O}_\uparrow(\omega_\mathrm{L})\mathrm{e}^{-\mathrm{i}\omega_\mathrm{L}t}\sigma_+ + \mathcal{O}_\downarrow(\omega_\mathrm{L})\mathrm{e}^{\mathrm{i}\omega_\mathrm{L}t}\sigma_-. \tag{2.9}$$

The components $\mathcal{O}_{\mathrm{o},z}$ are diagonal in spin space and have spin angular momentum $s_z = 0$, while correspondingly $\mathcal{O}_{\uparrow,\downarrow}$ are off-diagonal in spin space and have spin angular momentum $s_z = \pm 1$. In equation (2.9), we have used the definitions $\sigma_\pm = (\sigma_x \pm \mathrm{i}\sigma_y)/2$.

## 3. Andreev-reflection-induced spin torques

Quasi-particle scattering in a Josephson junction may lead to the formation of Andreev levels if the scattering occurs in such a way that the quasi-particles interfere constructively (figure 1*b*). In the presence of a precessing spin, the quasi-particle scattering is modified by processes shown in figure 1*c*; a tunnelling quasi-particle may gain (lose) energy $\omega_\mathrm{L}$ while simultaneously flipping its spin from down (up) to up (down). The Andreev level spectrum essentially depends on the ratio between the hopping amplitudes, $v_o/v_s$. If $v_o/v_s < (>)1$, the junction is in a $\pi$ (0) state [52,53] (figure 1*d*). The additional precession-induced tunnelling processes modify the Andreev levels. The Larmor frequency, $\omega_\mathrm{L}$, determines the amount of energy exchanged during a tunnelling event, while the cone angle, $\vartheta$, determines the amount of scattering between the spin-up and spin-down bands. These parameters, as well as the temperature, determine the population of the Andreev states [53,54]. In figure 2, we summarize how the tunnelling over a precessing spin modifies the Andreev spectra by introducing scattering resonances created by the combination of quanta exchange of $\hbar\omega_\mathrm{L}$ and spin flips. The charge current is time-independent but still dependent on both $\omega_\mathrm{L}$ and $\vartheta$ as seen in figure 2. While the Josephson effect over the precessing spin is interesting in its own right, we will not discuss the current–phase relations further in this paper and refer the interested reader to the original articles [52–54]. Instead, we will focus on the effects of dynamic spin-triplet correlations and their consequences.

An s-wave superconductor contains only spin-singlet correlations $\sim \frac{1}{2}\langle\psi_\uparrow\psi_\downarrow - \psi_\downarrow\psi_\uparrow\rangle$ and cannot support a spin current. Nevertheless, induced spin-triplet correlations can be formed due to spin mixing and locally broken spin-rotation symmetry [11,24,60]. The rotation of the classical spin generates new spinful correlations and spin currents that are created by the Andreev processes depicted in figure 1*b*,*c*; positive interference along closed loops leads to the spin-triplet correlations $\frac{1}{2}\langle\psi_\uparrow\psi_\downarrow + \psi_\downarrow\psi_\uparrow\rangle$, $\langle\psi_\uparrow\psi_\uparrow\rangle$ and $\langle\psi_\downarrow\psi_\downarrow\rangle$. These correlations depend on the characteristics of the tunnelling interface, i.e. the precession frequency, $\omega_\mathrm{L}$, the cone angle, $\vartheta$, the relative amplitude of hopping strengths, $v_o$, $v_s$, as well as the superconducting phase difference, $\varphi$, and the temperature, $T$. These spin-triplet correlations are localized near the junction interface and decay over length scales of the order of the superconducting coherence length [43,61].

The spin-singlet components can be quantified by

$$\psi(\hat{k}) = \int_{-\varepsilon_\mathrm{c}}^{\varepsilon_\mathrm{c}} \mathrm{d}\varepsilon\, [f^<(\hat{k},\varepsilon) + f^<(-\hat{k},\varepsilon)]/8\pi\mathrm{i},$$

where $f^<(\pm\hat{k},\varepsilon)$ denotes the anomalous Green's functions at the Fermi-surface points $\pm\hat{k}$. $\psi(\hat{k})$ is a measure of the (singlet) pairing correlations available to form a singlet order parameter $\Delta_s(\hat{k}) = \lambda_s\eta(\hat{k})\langle\eta(\hat{k}')\psi(\hat{k}')\rangle_{\hat{k}'\cdot\hat{n}>0}$, where $\eta(\hat{k}) = \eta(-\hat{k})$ are basis functions of even parity on which the pairing interaction may be expanded and $\hat{n}$ is the direction of the surface normal. The energy $\varepsilon_\mathrm{c}$ is the usual cut-off that appears in the BCS gap equation. The triplet correlations span the spin space

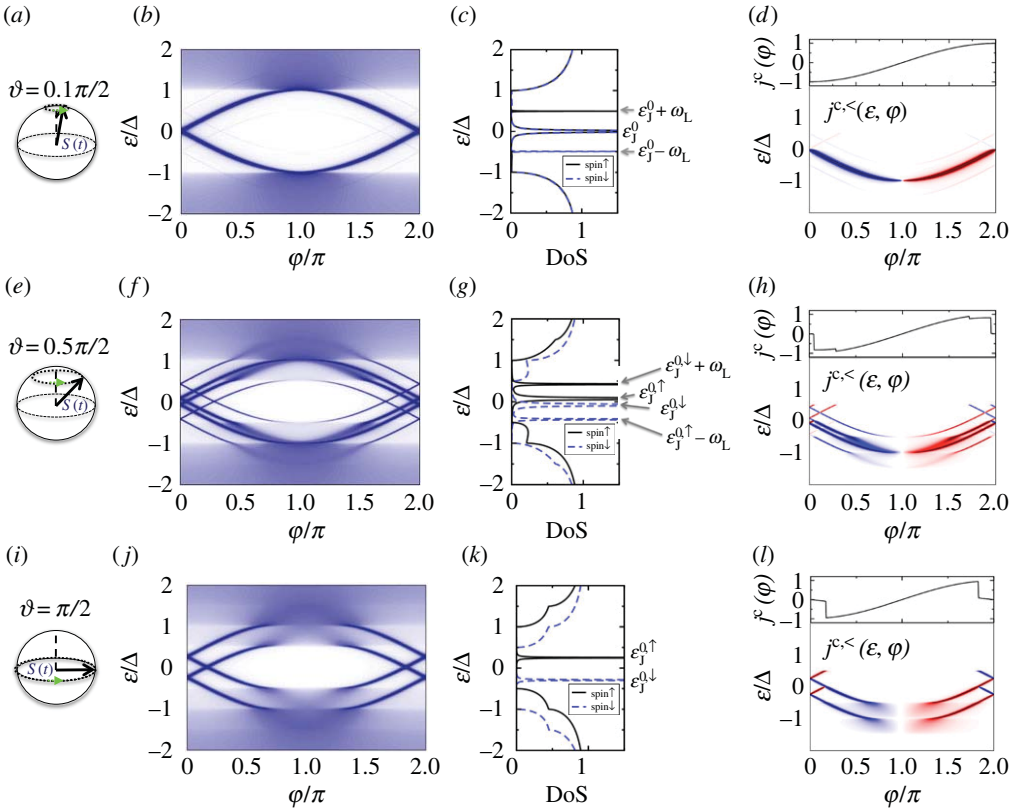


**Figure 2.** The Josephson effect over a precessing spin at frequency $\omega_L = 0.5\Delta$ for various cone angles (*a–d*) $\vartheta = 0.1\pi/2$, (*e–h*) $\vartheta = \pi/4$ and (*i–l*) $\vartheta = \pi/2$. The tunnelling parameters are $v_o = 0$, $v_s = 1$ and the temperature is $T = 10^{-5}\Delta$. The structure of the Andreev level spectrum is shown versus phase in (*b*, *f*, *j*) [59] and the density of states (DoS) at $\varphi = 0$ in (*c*, *g*, *k*) [53]. The current–phase relations, $j^c(\varphi)$, and the charge current kernels, $j^{c,<}(\varepsilon, \varphi)$, are shown in panels (*d*, *h*, *l*) [53]. The latter, $j^{c,<}(\varepsilon, \varphi)$, shows how the Andreev levels in (*b*, *f*, *j*) are populated and in which direction they carry current; red into the right $\partial\varepsilon/\partial\varphi > 0$ and blue into the left $\partial\varepsilon/\partial\varphi < 0$ lead. At some phase differences $\varphi_c < \varphi < 2\pi - \varphi_c$, scattering between the Andreev levels and the continuum states broadens the otherwise sharp in-gap states. The charge current (plotted in units of $e\Delta/\hbar$) is the energy-integrated spectral current and displays abrupt jumps at phase differences where Andreev levels become populated/unpopulated. The DoS at $\varphi = 0$ shows the splitting of the spin-up and spin-down Andreev levels as well as the scattering of the continuum levels into the gap. (Online version in colour.)

in such a way that $\boldsymbol{f}_z^< \sim \frac{1}{2}\langle\psi_\uparrow\psi_\downarrow + \psi_\downarrow\psi_\uparrow\rangle$ and $\boldsymbol{f}_{\uparrow/\downarrow}^< \sim \langle\psi_{\uparrow/\downarrow}\psi_{\uparrow/\downarrow}\rangle$. We quantify the induced spin-triplet correlations, $\boldsymbol{f}^<$, in terms of a $\boldsymbol{d}$ vector, which in general is a $2 \times 2$ triplet order parameter given by $\Delta_{\hat{k}} = \boldsymbol{d}(\hat{k}) \cdot \boldsymbol{\sigma}\, \mathrm{i}\sigma_y$ and points along the direction of zero spin projection of the Cooper pairs [62]. We make the following definitions:

$$\pi \text{ junctions} \quad \boldsymbol{d}_o(\hat{k}) = \hat{n} \cdot \hat{k} \int_{-\varepsilon_c}^{\varepsilon_c} \frac{\mathrm{d}\varepsilon}{8\pi\mathrm{i}} [\boldsymbol{f}^<(\hat{k}, \varepsilon) - \boldsymbol{f}^<(-\hat{k}, \varepsilon)] \tag{3.1a}$$

and

$$0 \text{ junctions} \quad \boldsymbol{d}_e(\hat{k}) = \int_{-\varepsilon_c}^{\varepsilon_c} \frac{\mathrm{d}\varepsilon}{8\pi\mathrm{i}} s_\varepsilon [\boldsymbol{f}^<(\hat{k}, \varepsilon) + \boldsymbol{f}^<(-\hat{k}, \varepsilon)], \tag{3.1b}$$

where the vector $\boldsymbol{d}_o$ is odd in momentum and even in energy, and the vector $\boldsymbol{d}_e$ is even in momentum and odd in energy; $s_\varepsilon$ is the sign of the energy $\varepsilon$. Spin-triplet pairing that is *even-in* $\hat{k}$ and *odd-in* $\varepsilon$ was first considered as a candidate pairing state for $^3$He [63] and has recently been realized in superconductor–inhomogeneous magnet interfaces [64]. The time dependence of

the $\boldsymbol{d}$ vector follows from equations (2.8) and (2.9), i.e.

$$\boldsymbol{d}(t) = \boldsymbol{d}_z + \boldsymbol{d}_\uparrow \, \mathrm{e}^{-\mathrm{i}\omega_\mathrm{L} t} + \boldsymbol{d}_\downarrow \, \mathrm{e}^{\mathrm{i}\omega_\mathrm{L} t}. \tag{3.2}$$

For $v_o = 0$ and finite $v_s$, the components are equal in magnitude, $\boldsymbol{d}_\uparrow = \boldsymbol{d}_\downarrow = -\boldsymbol{d}_z$, and scale with a common prefactor, $\mathcal{D}_s \omega_\mathrm{L}$, where $\mathcal{D}_s = 4{v_s}^2/[1 + 2({v_o}^2 + {v_s}^2) + ({v_o}^2 - {v_s}^2)^2]$. As expected, the $\boldsymbol{d}$-vector components decrease for increasing temperature until they vanish at $T = T_\mathrm{c}$. For finite values of $v_o$, the universal scaling disappears and the $\boldsymbol{d}$-vector components display an asymmetry between $\boldsymbol{d}_\uparrow$ and $\boldsymbol{d}_\downarrow$. For temperatures $T/T_\mathrm{c} \lesssim 0.1$, the $\boldsymbol{d}$ vector can be expressed in terms of the classical spin,

$$\boldsymbol{d}(t) = \delta_\mathrm{L} \dot{\boldsymbol{S}}(t) \times \boldsymbol{S}(t) + \delta_H (\gamma \boldsymbol{H}) \times \boldsymbol{S}(t) + \delta_z \boldsymbol{S}_z. \tag{3.3}$$

For the odd $\boldsymbol{d}$ vector, $\delta_{z,\mathrm{o}} = 0$ and, in the tunnel limit at zero temperature, $\delta_{\mathrm{L,o}} = \pi \mathcal{D}_s \sin(\varphi/2)$ and $\delta_{H,\mathrm{o}} = 4\pi \mathrm{i} v_o v_s \sin(\varphi/2)$. The $\boldsymbol{d}$ vectors in the left and right leads are related by $\boldsymbol{d}_\mathrm{R}(t) = -\boldsymbol{d}_\mathrm{L}(t)$.

The spin-vector part of the normal Green's function, $\boldsymbol{g}^{\mathrm{R/A}}$, can be expressed in terms of the spin-vector part of the anomalous Green's functions, $\boldsymbol{f}^{\mathrm{R/A}}$, using the normalization condition. In the limit of a small cone angle, the $z$-component is negligible and

$$\begin{aligned} g^{\mathrm{R(A)}}_{\uparrow/\downarrow,\alpha}\left(\varepsilon \mp \frac{\omega_\mathrm{L}}{2}\right) = \frac{1}{\bar{g}^{+/-,\mathrm{R(A)}}_{s,\alpha}} \Bigg\{ & \left[ \frac{(1 \pm \mathrm{i})}{2} f^{\mathrm{R(A)}}_{s,\alpha}\left(\varepsilon \pm \frac{\omega_\mathrm{L}}{2}\right) + \frac{(1 \mp \mathrm{i})}{2} f^{\mathrm{R(A)}}_{s,\alpha}(\varepsilon) \right] \tilde{f}^{\mathrm{R(A)}}_{\uparrow/\downarrow,\alpha}(\varepsilon) \\ & + \left[ \frac{(1 \mp \mathrm{i})}{2} \tilde{f}^{\mathrm{R(A)}}_{s,\alpha}\left(\varepsilon \pm \frac{\omega_\mathrm{L}}{2}\right) + \frac{(1 \pm \mathrm{i})}{2} \tilde{f}^{\mathrm{R(A)}}_{s,\alpha}(\varepsilon) \right] f^{\mathrm{R(A)}}_{\uparrow/\downarrow,\alpha}(\varepsilon) \Bigg\}, \end{aligned} \tag{3.4}$$

where $\bar{g}^{+/-,\mathrm{R(A)}}_{s,\alpha} = g^{\mathrm{R(A)}}_{s,\alpha}(\varepsilon) + g^{\mathrm{R(A)}}_{s,\alpha}(\varepsilon \pm \omega_\mathrm{L}/2)$ and $g^{\mathrm{R(A)}}_{x,\alpha} = [g^{\mathrm{R(A)}}_{\uparrow,\alpha} + g^{\mathrm{R(A)}}_{\downarrow,\alpha}]/2$ and $g^{\mathrm{R(A)}}_{y,\alpha} = \mathrm{i}[g^{\mathrm{R(A)}}_{\uparrow,\alpha} - g^{\mathrm{R(A)}}_{\downarrow,\alpha}]/2$.

It is then clear that the existence of the spin currents, $j^\mathrm{s}_\alpha = \frac{1}{4}\int (\mathrm{d}\varepsilon/8\pi\mathrm{i}) \, \mathrm{Tr}\{\hat{\tau}_3 \hat{\boldsymbol{\sigma}} [\hat{g}^{\mathrm{i,K}}_\alpha(\varepsilon, t) - \hat{g}^{\mathrm{o,K}}_\alpha(\varepsilon, t)]\}$, is a direct consequence of the precession-induced spin-triplet correlations; see also Appendix in [54]. Unfortunately, the spin currents decay over relatively short distances, *viz.* the superconducting coherence length, and are therefore difficult to measure. The spin current is nothing but transport of spin angular momentum and the non-conservation of the spin current results in a torque acting on the rotating spin, thereby creating a back-action on the precessing spin that is sufficiently large for experimental detection [53], as will be described below.

Since $j^\mathrm{s}_\mathrm{R}(t, \varphi) = -j^\mathrm{s}_\mathrm{L}(t, -\varphi) \neq j^\mathrm{s}_\mathrm{L}(t, \varphi)$, the difference between the spin currents can be used to calculate the torque $\boldsymbol{\tau}(t)$ in equation (2.1). We call this torque the Andreev torque since it has its origin in the Andreev scattering processes described in figure 1. The torque contribution per conduction channel is

$$\boldsymbol{\tau}_A(t) = \frac{2\hbar}{S} \mathcal{D}_s \beta_H \cos\vartheta \, (\gamma \boldsymbol{H}) \times \boldsymbol{S}(t). \tag{3.5}$$

This torque describes a shift of the precession frequency, $\omega_\mathrm{L} \to \omega_\mathrm{L}[1 + (2\hbar/S)\mathcal{D}_s \beta_H \cos\vartheta]$, and this shift is, therefore, a direct consequence of the induced spin-triplet correlations.

A measurement of this frequency shift is a measurement of the induced spin-triplet correlations. Since the shift is $\propto 1/S$, we suggest a nanomagnet with a spin that is small, but still large enough to be treated as a classical spin, say a magnetic nanoparticle with spin $S \sim 50\hbar$. For a contact with two superconducting niobium (Nb) leads, the effective contact area is approximately $\pi \xi_0^2$, where the superconducting coherence length $\xi_0 \sim 40\,\mathrm{nm}$ for Nb. A contact width of approximately 40 nm contains $n \sim 200$ conduction channels. In bulk Nb, $\Delta \sim 1\,\mathrm{meV}$, but can be made considerably smaller in the point contact, say $\Delta \sim 200\,\mu\mathrm{eV}$. We can now study the changes to the precession due to the Andreev torque. In a typical ferromagnetic resonance (FMR) experiment, the resonance peak in the power absorption spectrum has a width that is produced by inhomogeneous broadening, e.g. from anisotropy fields, and homogeneous broadening, which is due to Gilbert damping, and can be expressed as $\Delta H_\mathrm{hom} = (2/\sqrt{3}) H \alpha_\mathrm{G}$ [65], where $H = |\boldsymbol{H}|$ and $\alpha_\mathrm{G} = (2\hbar/S) n \alpha \mathcal{D}_s$ is the Gilbert constant [30]. A typical magnetic field is $H \sim 180\,\mathrm{mT}$, which corresponds to a Larmor precession of approximately $20\,\mu\mathrm{eV}$ or $5\,\mathrm{GHz}$. Here,

we have assumed a uniform precessional motion. In [53], it was shown that the normal quasiparticles freeze out as the temperature is lowered. This process results in a decrease of the width of the resonance peak [66]. For a junction with $\mathcal{D}_s \sim 0.1$, the difference in homogeneous broadening is of the order of $\Delta H_{\rm hom}(T/T_{\rm c} > 1) - \Delta H_{\rm hom}(T/T_{\rm c} \to 0) \sim 80\,{\rm mT}$. In addition to the resonance peak width reduction, the shift of the resonance peak $H_0$ due to the Andreev torque appears. The frequency shift corresponds to $\Delta\omega_{\rm L}/\omega_{\rm L} = \alpha_G \beta_H \cos\vartheta$. In the tunnel limit, $\beta_H \sim \frac{1}{16}(\omega_{\rm L}/\Delta)$ in the low-temperature limit [53]. In this limit, a spin with angle $\vartheta = \pi/4$ can hence generate a displacement of the resonance peak by $\Delta H_0/H_0 \sim 2\%$. By increasing the junction transparency, the ratio $\hbar n/S$, or the ratio $\omega_{\rm L}/\Delta$, the ratio $\Delta H_0/H_0$ can be improved.

## 4. Spin-precession-assisted multiple Andreev reflection

Replacing the phase bias by a voltage bias (figure 3*a*) leads to several new features [55] attributable to the interplay between the time-dependent $\boldsymbol{d}$ vectors and the Josephson frequency, $\omega_{\rm J} = 2\,{\rm eV}/\hbar$. The replacement causes the phase difference to increase linearly in time, $\varphi(t) = \varphi_0 + \omega_{\rm J} t$, where $\varphi_0$ is the initial phase difference. The bias voltage in combination with energy exchange with the precessing spin creates multiple Andreev reflection (MAR) processes that lead to characteristic signatures in the charge current–voltage ($I$–$V$) characteristics [47,67–69]. Two examples of spin-precession-assisted MAR are shown in figure 3. Similar to the phase-biased case, energy absorption (emission) corresponds to spin flip from down (up) to up (down). The first-order process shown in figure 3*b*, which includes an energy absorption of $\omega_{\rm L}$, leads to a contribution to the $I$–$V$ characteristics at the energy $eV = 2\Delta - \omega_{\rm L}$. Figure 3*c* shows the two possible second-order processes that include absorption of energy. The spin flip associated with the energy exchange introduces a minus sign in the next Andreev-reflection amplitude due to the change between the spinors $(\psi_\uparrow, \psi_\downarrow^\dagger)^{\rm T} \leftrightarrow (\psi_\downarrow, \psi_\uparrow^\dagger)^{\rm T}$. This sign difference leads to destructive interference and suppression of the total Andreev reflection. Destructive interference occurs for all even processes, $n = 2, 4, \ldots$, while higher-order odd processes display constructive interference.

The bias voltage makes the calculations of the charge and spin currents considerably more complicated. This complication arises in large part due to the MAR processes, which make it impossible to express Green's functions using a closed set of equations. Instead, a recursive approach (see [55] for details) has to be used. The general time dependence of a general matrix such as $\check{X}(t, t')$ in equation (2.8) now has to be complemented by the time dependence generated by the Josephson frequency. In general, the current is given by

$$j_\alpha^\mu(t) = \sum_{n,m} {\rm e}^{-{\rm i}(n\varphi_0 + m\chi_0) - {\rm i}(n\omega_{\rm J} + m\omega_{\rm L})t} (j_\alpha^\mu)_n^m. \tag{4.1}$$

The current components are

$$(j_\alpha^\mu)_n^m = \int \frac{{\rm d}\varepsilon}{4} {\rm Tr}\{\hat{\kappa}^\mu [\check{t}(\varepsilon + n\omega_{\rm J} + m\omega_{\rm L})\check{g}(\varepsilon) - \check{g}(\varepsilon + n\omega_{\rm J} + m\omega_{\rm L})\check{t}(\varepsilon + n\omega_{\rm J} + m\omega_{\rm L})]^<\}, \tag{4.2}$$

where we have defined $\hat{\kappa}^0 = e\hat{\tau}_3$ for the charge current and $\hat{\kappa}^i = {\rm diag}(\sigma_i, \sigma_y\sigma_i\sigma_y)/2$ for a spin current with a polarization in the $i = x, y, z$ direction. Note that just as the current depends on the initial phase $\varphi_0$, it also depends on $\chi_0$, which is the initial value of the in-plane projection of the precessing spin. The integer $m$ takes the values $\{-1, 0, 1\}$ corresponding to $\{\downarrow, d, \uparrow\}$ in equation (2.8). Defining $v_{\uparrow/\downarrow} = v_o \pm v_s \cos\vartheta$, we write $\mathcal{D}_{\uparrow(\downarrow)} = 4v_{\uparrow(\downarrow)}^2/[1 + v_{\uparrow(\downarrow)}^2]^2$.

The DC charge current and the differential conductance, plotted in figure 3*d*, clearly show the contributions to the current generated by the spin-precession-assisted MAR processes. These features appear at voltages $eV = (2\Delta \pm \omega_{\rm L})/n$, where $n = 1, 3, \ldots$. Note that, as expected, the contributions for the even processes $n = 2, 4, \ldots$ are absent. It can be shown that the AC charge current only includes harmonics of $\omega_{\rm J}$, i.e. $j_\alpha^0(t) = \sum_n {\rm e}^{-{\rm i}n(\varphi_0 + \omega_{\rm J} t)} (j_\alpha^0)_n^0$. This time dependence is an effect of the combined energy exchange spin-flip tunnelling processes.

The spin current, on the other hand, includes all harmonics of the Larmor and Josephson frequencies. This time dependence is captured by the spin-transfer torque, whose $\omega_{\rm L}$ dependence

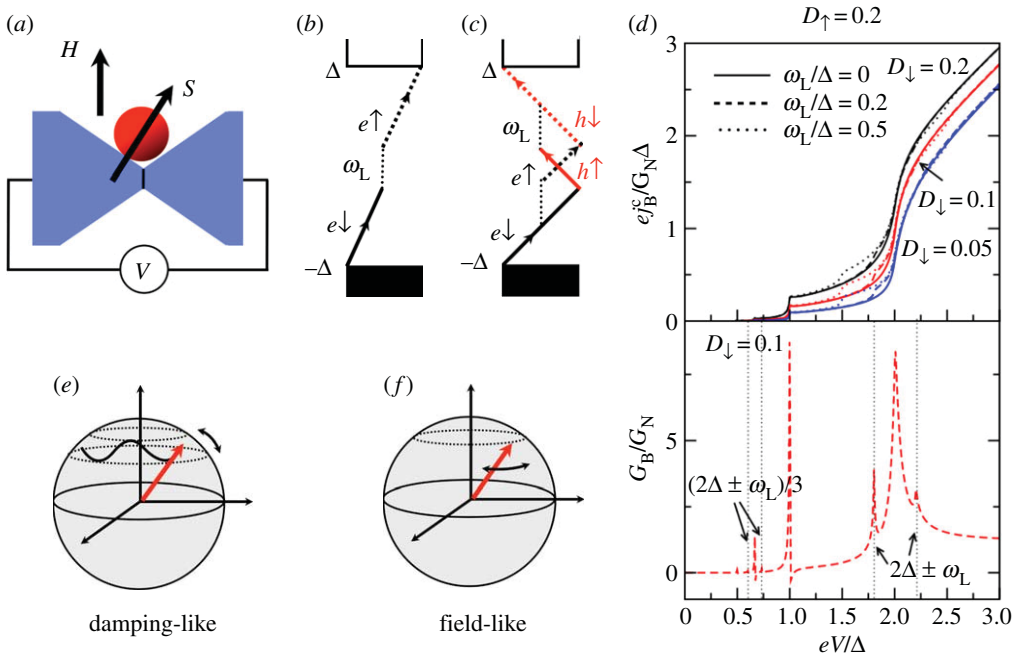


**Figure 3.** (*a*) Same set-up as in figure 1 but with a bias voltage applied across the tunnel junction. The (*b*) first- and (*c*) second-order MAR processes combined with absorption of energy $\omega_L$. (*d*) Current–voltage characteristics for the DC charge current $j_B^c$ (top) and differential conductance (bottom), $G_B = \partial j_B^c/\partial V$, normalized by the normal conductance $G_N = [e^2/h][\mathcal{D}_\uparrow + \mathcal{D}_\downarrow]$. In both plots, $\vartheta = \pi/8$. Sketches of the time-dependent (*e*) damping-like and (*f*) field-like torques created by spin-precession-assisted MAR. (Online version in colour.)

is described by the expression

$$\boldsymbol{\tau}(t) = \frac{\gamma_H(t)}{S}\gamma \boldsymbol{H} \times \boldsymbol{S} + \frac{\gamma_L(t)}{S^2}\dot{\boldsymbol{S}} \times \boldsymbol{S}, \tag{4.3}$$

where the prefactors, $\gamma_{H/L}$, oscillate with the Josephson frequency, $\gamma_{H/L}(t) = \sum_n \gamma_{H/L,n}\, e^{in\omega_J t}$. The component $\gamma_{L,0}$ describes a finite shift of the precession angle $\vartheta$, while the term $\propto \gamma_{H,0}$ signals a shift of the precession frequency. The damping-like torque $\propto \gamma_{L,n}$ and the field-like torque $\propto \gamma_{H,n}$ describe Josephson nutations [70] and oscillations of the precession frequency, respectively.

Since the torque (4.3) includes harmonics of both $\omega_J$ and $\omega_L$, resonances may occur when the two frequencies are commensurate. These Shapiro resonances occur at the bias voltage $V_n^m = -(m/n)\omega_L/2e$ where $n, m \neq 0$, and this results in a DC contribution to the spin-transfer torque and can be seen as a rectification of the higher harmonics of the torque in §3. As the AC part of the torque (4.3) originates from an in-plane spin-polarized current, one can then conclude that the Shapiro resonances produce DC in-plane torque components. The Shapiro resonances hence break the rotational symmetry around the $z$-axis and, therefore, the Shapiro torque depends on the initial angle of the nanomagnet's magnetization direction, $\chi_0$. This situation is analogous to the $\varphi_0$ dependence for the Shapiro steps seen in microwave-irradiated Josephson junctions [71–73].

The DC Shapiro torque will cause the spin to precess around a new $z$-axis. Choosing suitable parameters and applying a self-consistent solution, one finds that the Shapiro torque is able to reverse the spin's direction. To this end, we choose $n = 1$ and optimize the effect of the Shapiro torque by maximizing the ratio $\gamma_{H,1}/\gamma_{L,1}$. It was found in [55] that $\gamma_{H,1}$ strongly depends on the junction transparency but exhibits a weak dependence on the precession angle. We, therefore, choose $v_o = 0$, $v_s = 0.7$ and $\vartheta = 0.1\pi$. We consider a tunnel junction consisting of Nb having a superconducting gap $\Delta \sim 0.5\,\text{meV}$ and containing a magnetic nanoparticle with spin $S \sim 50\hbar$

with a typical frequency $\omega_L \sim 5$ GHz that corresponds to a magnetic field well below the critical magnetic field. We therefore have $\omega_L/\Delta = 0.01$. A magnetic field close to the critical magnetic field reduces $\Delta$ and increases the resolution of features depending on the ratio $\omega_L/\Delta$, e.g. the subgap features in the DC charge current. A point contact of width approximately 40 nm has approximately 200 conduction channels, which gives an estimated sub-nanosecond switching time for the first Shapiro resonance.

## 5. Conclusion

We have reviewed recent work on how the magnetization dynamics of a nanomagnet couple to the charge and spin Josephson effects. The precession of the nanomagnet modifies the Andreev scattering in several ways. First, it introduces a spin-polarized Andreev level spectrum and dynamical spin-triplet pairing correlations in the vicinity of the junction. Second, it couples in-gap Andreev levels with the continuum part of the spectrum, causing a non-equilibrium population of the Andreev levels. Third, it creates a non-equilibrium population of the Andreev levels, leading to Andreev levels carrying current in opposite directions being populated and a strongly modified current–phase relation. We have focused on the consequences of the spin-polarized Andreev level spectra and how they couple back to the precession dynamics of the nanomagnet via conservation of spin angular momentum. Depending on whether the Josephson junction is phase biased or voltage biased, this torque can modify the precession frequency, either by a frequency shift or by frequency modulations, or it can introduce nutations. Recent experiments on superconductor–ferromagnet nanojunctions can extract the microscopic details of the scattering and match junction parameters such as spin-filtering and spin-mixing effects [74–76]. If the ferromagnetic part of the junction were a single-domain magnetic grain, properties described in this review could be probed in experiments.

Data accessibility. This article has no additional data.

Competing interests. We declare we have no competing interests.

Funding. C.H. and W.B. were supported by the DFG and SFB 767. M.F. acknowledges support from the Swedish Research Council (VR).

## References

1. Eschrig M. 2011 Spin-polarized supercurrents for spintronics. *Phys. Today* **64**, 43. (doi:10.1063/1.3541944)
2. Linder J, Robinson JWA. 2015 Superconducting spintronics. *Nat. Phys.* **11**, 307–315. (doi:10.1038/nphys3242)
3. Bulaevskii LN, Kuzii VV, Sobyanin AA. 1977 Superconducting system with weak links and current in the ground state. *Zh. Éksp. Teor. Fiz.* **25**, 314. [*JETP Lett.* **25**, 290].
4. Ryazanov VV, Oboznov VA, Rusanov AYu, Veretennikov AV, Golubov AA, Aarts J. 2001 Coupling of two superconductors through a ferromagnet: evidence for a $\pi$-junction. *Phys. Rev. Lett.* **86**, 2427–2430. (doi:10.1103/PhysRevLett.86.2427)
5. Kontos T, Aprili M, Lesueur J, Genêt F, Stephanidis B, Boursier R. 2002 Josephson junction through a thin ferromagnetic layer: negative coupling. *Phys. Rev. Lett.* **89**, 137007. (doi:10.1103/PhysRevLett.89.137007)
6. Buzdin AI. 2005 Proximity effects in superconductor–ferromagnet heterostructures. *Rev. Mod. Phys.* **77**, 935–976. (doi:10.1103/RevModPhys.77.935)
7. Bergeret FS, Volkov AF, Efetov KB. 2001 Enhancement of the Josephson current by an exchange field in superconductor–ferromagnet structures. *Phys. Rev. Lett.* **86**, 3140–3143. (doi:10.1103/PhysRevLett.86.3140)
8. Bergeret FS, Volkov AF, Efetov KB. 2005 Odd triplet superconductivity and related phenomena in superconductor–ferromagnet structures. *Rev. Mod. Phys.* **77**, 1321–1373. (doi:10.1103/RevModPhys.77.1321)
9. Houzet M, Buzdin AI. 2007 Long range triplet Josephson effect through a ferromagnetic trilayer. *Phys. Rev. B* **76**, 060504(R). (doi:10.1103/PhysRevB.76.060504)

10. Braude V, Nazarov Yu. V. 2007 Fully developed triplet proximity effect. *Phys. Rev. Lett.* **98**, 077003. (doi:10.1103/PhysRevLett.98.077003)
11. Eschrig M, Löfwander T. 2008 Triplet supercurrents in clean and disordered half-metallic ferromagnets. *Nat. Phys.* **4**, 138–143. (doi:10.1038/nphys831)
12. Keizer RS, Goennenwein STB, Klapwijk TM, Miao G, Xiao G, Gupta A. 2006 A spin triplet supercurrent through the half-metallic ferromagnet $CrO_2$. *Nature* **439**, 825–827. (doi:10.1038/nature04499)
13. Khaire TS, Khasawneh MA, Pratt Jr WP, Birge NO. 2010 Observation of spin-triplet superconductivity in Co-based Josephson junctions. *Phys. Rev. Lett.* **104**, 137002. (doi:10.1103/PhysRevLett.104.137002)
14. Konschelle F, Buzdin A. 2009 Magnetic moment manipulation by a Josephson current. *Phys. Rev. Lett.* **102**, 017001. (doi:10.1103/PhysRevLett.102.017001)
15. Mai S, Kandelaki E, Volkov AF, Efetov KB. 2011 Interaction of Josephson and magnetic oscillations in Josephson tunnel junctions with a ferromagnetic layer. *Phys. Rev. B* **84**, 144519. (doi:10.1103/PhysRevB.84.144519)
16. Cai L, Chudnovsky EM. 2010 Interaction of a nanomagnet with a weak superconducting link. *Phys. Rev. B* **82**, 104429. (doi:10.1103/PhysRevB.82.104429)
17. Waintal X, Brouwer PW. 2001 Current-induced switching of magnetic domains to a perpendicular configuration. *Phys. Rev. B* **63**, R220407. (doi:10.1103/PhysRevB.63.220407)
18. Waintal X, Brouwer PW. 2002 Magnetic exchange interaction induced by a Josephson current. *Phys. Rev. B* **65**, 054407. (doi:10.1103/PhysRevB.65.054407)
19. Michelsen J, Shumeiko VS, Wendin G. 2008 Manipulation with Andreev states in spin active mesoscopic Josephson junctions. *Phys. Rev. B* **77**, 184506. (doi:10.1103/PhysRevB.77.184506)
20. Linder J, Yokoyama T. 2011 Supercurrent-induced magnetization dynamics in a Josephson junction with two misaligned ferromagnetic layers. *Phys. Rev. B* **83**, 012501. (doi:10.1103/PhysRevB.83.012501)
21. Kulagina I, Linder J. 2014 Spin supercurrent, magnetization dynamics, and $\varphi$-state in spin-textured Josephson junctions. *Phys. Rev. B* **90**, 054504. (doi:10.1103/PhysRevB.90.054504)
22. Zhu J-X, Nussinov Z, Shnirman A, Balatsky AV. 2004 Novel spin dynamics in a Josephson junction. *Phys. Rev. Lett.* **92**, 107001. (doi:10.1103/PhysRevLett.92.107001)
23. Zhao E, Sauls JA. 2008 Theory of nonequilibrium spin transport and spin–transfer torque in superconducting–ferromagnetic nanostructures. *Phys. Rev. B* **78**, 174511. (doi:10.1103/PhysRevB.78.174511)
24. Houzet M. 2008 Ferromagnetic Josephson junction with precessing magnetization. *Phys. Rev. Lett.* **101**, 057009. (doi:10.1103/PhysRevLett.101.057009)
25. Braude V, Blanter Ya. M. 2008 Triplet Josephson effect with magnetic feedback in a superconductor–ferromagnet heterostructure. *Phys. Rev. Lett.* **100**, 207001. (doi:10.1103/PhysRevLett.100.207001)
26. Yokoyama T, Tserkovnyak Y. 2009 Tuning odd triplet superconductivity by spin pumping. *Phys. Rev. B* **80**, 104416. (doi:10.1103/PhysRevB.80.104416)
27. Shomali Z, Zareyan M, Belzig W. 2011 Spin supercurrent in Josephson contacts with noncollinear ferromagnets. *New J. Phys.* **13**, 083033. (doi:10.1088/1367-2630/13/8/083033)
28. Petković I, Aprili M, Barnes SE, Beuneu F, Maekawa S. 2009 Direct dynamical coupling of spin modes and singlet Josephson supercurrent in ferromagnetic Josephson junctions. *Phys. Rev. B* **80**, 220502. (doi:10.1103/PhysRevB.80.220502)
29. Barnes SE, Aprili M, Petković I, Maekawa S. 2011 Ferromagnetic resonance with a magnetic Josephson junction. *Supercond. Sci. Technol.* **24**, 024020. (doi:10.1088/0953-2048/24/2/024020)
30. Gilbert TL. 2004 A phenomenological theory of damping in ferromagnetic materials. *IEEE Trans. Magn.* **40**, 3443–3449. (doi:10.1109/TMAG.2004.836740)
31. Tserkovnyak Y, Brataas A, Bauer GEW, Halperin BI. 2005 Nonlocal magnetization dynamics in ferromagnetic heterostructures. *Rev. Mod. Phys.* **77**, 1375–1421. (doi:10.1103/RevModPhys.77.1375)
32. Zhu J-X, Balatsky AV. 2003 Josephson current in the presence of a precessing spin. *Phys. Rev. B* **67**, 174505. (doi:10.1103/PhysRevB.67.174505)
33. Eilenberger G. 1968 Transformation of Gorkov's equation for type II superconductors into transport-like equations. *Z. Phys.* **214**, 195–213. (doi:10.1007/BF01379803)
34. Larkin AI, Ovchinnikov YN. 1969 Quasiclassical method in the theory of superconductivity. *Zh. Éksp. Teor. Fiz.* **55**, 2262. [*Sov. Phys. JETP* **28**, 1200].

35. Eliashberg GM. 1971 Inelastic electron collisions and nonequilibrium stationary states in superconductors. *Zh. Éksp. Teor. Fiz.* **61**, 1254. [*Sov. Phys. JETP* **34**, 668 (1972)].
36. Serene JW, Rainer D. 1983 The quasiclassical approach to superfluid $^3$He. *Phys. Rep.* **101**, 221–311. (doi:10.1016/0370-1573(83)90051-0)
37. Zaitsev AV. 1984 Quasiclassical equations of the theory of superconductivity for contiguous metals and the properties of constricted microcontacts. *Zh. Éksp. Teor. Fiz.* **86**, 1742. [*Sov. Phys. JETP* **59**, 1015].
38. Shelankov AL. 1984 2-particle tunnelling in normal metal–superconductor contact. *Sov. Phys. Solid State* **26**, 981–990.
39. Millis AJ, Rainer D, Sauls JA. 1988 Quasiclassical theory of superconductivity near magnetically active interfaces. *Phys. Rev. B* **38**, 4504–4515. (doi:10.1103/PhysRevB.38.4504)
40. Nagai K, Hara J. 1988 Boundary conditions for quasiclassical Green's function for superfluid Fermi systems. *J. Low Temp. Phys.* **71**, 351–367. (doi:10.1007/BF00116868)
41. Eschrig M. 2000 Distribution functions in nonequilibrium theory of superconductivity and Andreev spectroscopy in unconventional superconductors. *Phys. Rev. B* **61**, 9061–9076. (doi:10.1103/PhysRevB.61.9061)
42. Shelankov A, Ozana M. 2000 Quasiclassical theory of superconductivity: a multiple-interface geometry. *Phys. Rev. B* **61**, 7077–7100. (doi:10.1103/PhysRevB.61.7077)
43. Fogelström M. 2000 Josephson currents through spin-active interfaces. *Phys. Rev. B* **62**, 11 812–11 819. (doi:10.1103/PhysRevB.62.11812)
44. Barash YS, Bobkova IV, Kopp T. 2002 Josephson current in S–FIF–S junctions: nonmonotonic dependence on misorientation angle. *Phys. Rev. B* **66**, 140503(R). (doi:10.1103/PhysRevB.66.140503)
45. Zhao E, Löfwander T, Sauls JA. 2004 Nonequilibrium superconductivity near spin-active interfaces. *Phys. Rev. B* **70**, 134510. (doi:10.1103/PhysRevB.70.134510)
46. Eschrig M. 2009 Scattering problem in nonequilibrium quasiclassical theory of metals and superconductors: general boundary conditions and applications. *Phys. Rev. B* **80**, 134511. (doi:10.1103/PhysRevB.80.134511)
47. Cuevas JC, Martín-Rodero A, Levy Yeyati A. 1996 Hamiltonian approach to the transport properties of superconducting quantum point contacts. *Phys. Rev. B* **54**, 7366–7379. (doi:10.1103/PhysRevB.54.7366)
48. Cuevas JC, Fogelström M. 2001 Quasiclassical description of transport through superconducting contacts. *Phys. Rev. B* **64**, 104502. (doi:10.1103/PhysRevB.64.104502)
49. Andersson M, Cuevas JC, Fogelström M. 2002 Transport through superconductor/magnetic dot/superconductor structures. *Physica C* **367**, 117–122. (doi:10.1016/S0921-4534(01)00977-7)
50. Eschrig M, Kopu J, Cuevas JC, Schön G. 2003 Theory of half-metal/superconductor heterostructures. *Phys. Rev. Lett.* **90**, 137003. (doi:10.1103/PhysRevLett.90.137003)
51. Kopu J, Eschrig M, Cuevas JC, Fogelström M. 2004 Transfer-matrix description of heterostructures involving superconductors and ferromagnets. *Phys. Rev. B* **69**, 094501. (doi:10.1103/PhysRevB.69.094501)
52. Teber S, Holmqvist C, Fogelström M. 2010 Transport and magnetization dynamics in a superconductor/single-molecule magnet/superconductor junction. *Phys. Rev. B* **81**, 174503. (doi:10.1103/PhysRevB.81.174503)
53. Holmqvist C, Teber S, Fogelström M. 2011 Nonequilibrium effects in a Josephson junction coupled to a precessing spin. *Phys. Rev. B* **83**, 104521. (doi:10.1103/PhysRevB.83.104521)
54. Holmqvist C, Belzig W, Fogelström M. 2012 Spin-precession-assisted supercurrent in a superconducting quantum point contact coupled to a single-molecule magnet. *Phys. Rev. B* **86**, 054519. (doi:10.1103/PhysRevB.86.054519)
55. Holmqvist C, Fogelström M, Belzig W. 2014 Spin-polarized Shapiro steps and spin-precession-assisted multiple Andreev reflection. *Phys. Rev. B* **90**, 014516. (doi:10.1103/PhysRevB.90.014516)
56. Buchholtz LJ, Rainer D. 1979 Quasiclassical boundary conditions for Fermi liquids at surfaces. *Z. Phys. B* **35**, 151–162. (doi:10.1007/BF01321241)
57. Thuneberg EV, Kurkijärvi J, Rainer D. 1981 Quasiclassical theory of ions in $^3$He. *J. Phys. C* **14**, 5615–5624. (doi:10.1088/0022-3719/14/36/006)
58. Thuneberg EV, Kurkijärvi J, Rainer D. 1984 Elementary-flux-pinning potential in type-II superconductors. *Phys. Rev. B* **29**, 3913–3923. (doi:10.1103/PhysRevB.29.3913)

59. Holmqvist C. 2010 Non-equilibrium effects in nanoscale superconducting hybrid junctions. PhD thesis, Chalmers University of Technology.
60. Alidoust M, Linder J, Rashedi G, Yokoyama T, Sudbø A. 2010 Spin-polarized Josephson current in superconductor/ferromagnet/superconductor junctions with inhomogeneous magnetization. *Phys. Rev. B* **81**, 014512. (doi:10.1103/PhysRevB.81.014512)
61. Shevtsov O, Löfwander T. 2014 Spin imbalance in hybrid superconducting structures with spin-active interfaces. *Phys. Rev. B* **90**, 085432. (doi:10.1103/PhysRevB.90.085432)
62. Vollhardt D, Wölfle P. 1990 *The superfluid phases of helium 3*. London, UK: Taylor and Francis.
63. Berezinskii VL. 1974 New model of anisotropic phase of superfluid He-3. *Pis'ma Zh. Eksp. Teor. Fiz.* **20**, 628. [*JETP Lett.* **20**, 287].
64. DiBernardo A, Diesch S, Gu Y, Linder J, Divitini G, Ducati C, Scheer E, Blamire MG, Robinson JWA. 2015 Signature of magnetic-dependent gapless odd frequency states at superconductor/ferromagnet interfaces. *Nat. Commun.* **6**, 8053. (doi:10.1038/ncomms9053)
65. Platow W, Anisimov AN, Dunifer GL, Farle M, Baberschke K. 1998 Correlations between ferromagnetic-resonance linewidths and sample quality in the study of metallic ultrathin films. *Phys. Rev. B* **58**, 5611–5621. (doi:10.1103/PhysRevB.58.5611)
66. Bell C, Milikisyants S, Huber M, Aarts J. 2008 Spin dynamics in a superconductor–ferromagnet proximity system. *Phys. Rev. Lett.* **100**, 047002. (doi:10.1103/PhysRevLett.100.047002)
67. Octavio M, Tinkham M, Blonder GE, Klapwijk TM. 1983 Subharmonic energy-gap structure in superconducting constrictions. *Phys. Rev. B* **27**, 6739–6746. (doi:10.1103/PhysRevB.27.6739)
68. Bratus EN, Shumeiko VS, Wendin G. 1995 Theory of subharmonic gap structure in superconducting mesoscopic tunnel contacts. *Phys. Rev. Lett.* **74**, 2110–2113. (doi:10.1103/PhysRevLett.74.2110)
69. Averin D, Bardas A. 1995 AC Josephson effect in a single quantum channel. *Phys. Rev. Lett.* **75**, 1831–1834. (doi:10.1103/PhysRevLett.75.1831)
70. Nussinov Z, Shnirman A, Arovas DP, Balatsky AV, Zhu JX. 2005 Spin and spin-wave dynamics in Josephson junctions. *Phys. Rev. B* **71**, 214520. (doi:10.1103/PhysRevB.71.214520)
71. Cuevas JC, Heurich J, Martín-Rodero A, Levy Yeyati A, Schön G. 2002 Subharmonic Shapiro steps and assisted tunneling in superconducting point contacts. *Phys. Rev. Lett.* **88**, 157001. (doi:10.1103/PhysRevLett.88.157001)
72. Uzawa Y, Wang Z. 2005 Coherent multiple charge transfer in a superconducting NbN tunnel junction. *Phys. Rev. Lett.* **95**, 017002. (doi:10.1103/PhysRevLett.95.017002)
73. Chauvin M, vom Stein P, Pothier H, Joyez P, Huber ME, Esteve D, Urbina C. 2006 Superconducting atomic contacts under microwave irradiation. *Phys. Rev. Lett.* **97**, 067006. (doi:10.1103/PhysRevLett.97.067006)
74. Quay CHL, Chevallier D, Bena C, Aprili M. 2013 Spin imbalance and spin-charge separation in a mesoscopic superconductor. *Nat. Phys.* **9**, 84–88. (doi:10.1038/nphys2518)
75. Hübler F, Wolf MJ, Beckmann D, von Löhneysen H. 2012 Long-range spin-polarized quasiparticle transport in mesoscopic Al superconductors with a Zeeman splitting. *Phys. Rev. Lett.* **109**, 207001. (doi:10.1103/PhysRevLett.109.207001)
76. Wolf MJ, Hübler F, Kolenda S, von Löhneysen H, Beckmann D. 2013 Spin injection from a normal metal into a mesoscopic superconductor. *Phys. Rev. B* **87**, 024517. (doi:10.1103/PhysRevB.87.024517)